





## Article

# Enhancement of the Shielding Capability of Soda–Lime Glasses with $\text{Sb}_2\text{O}_3$ Dopant: A Potential Material for Radiation Safety in Nuclear Installations

M.I. Sayyed <sup>1,2</sup> , K.A. Mahmoud <sup>3,4,\*</sup> , O.L. Tashlykov <sup>3</sup>, Mayeen Uddin Khandaker <sup>5,\*</sup>  and M.R.I. Faruque <sup>6</sup> 

<sup>1</sup> Department of physics, Faculty of Science, Isra University, Amman 11622, Jordan; mabualssayed@ut.edu.sa

<sup>2</sup> Department of Nuclear Medicine Research, Institute for Research and Medical Consultations, Imam Abdulrahman bin Faisal University, Dammam 31441, Saudi Arabia

<sup>3</sup> Department of Nuclear Power Plants and Renewable Energy Sources, Ural Power Engineering Institute, Ural Federal University, St. Mira, 19, 620002 Yekaterinburg, Russia; otashlykov@list.ru

<sup>4</sup> Nuclear Materials Authority, Maadi, Cairo 11381, Egypt

<sup>5</sup> Center for Applied Physics and Radiation Technologies, School of Engineering and Technology, Sunway University, Bandar Sunway, Selangor 47500, Malaysia

<sup>6</sup> Space Science Centre (ANGKASA), Universiti Kebangsaan Malaysia, Bangi 43600, Malaysia; rashed@ukm.edu.my

\* Correspondence: kmakhmud@urfu.ru (K.A.M.); mayeenk@sunway.edu.my (M.U.K.)

**Abstract:** Elastic moduli were theoretically computed using the Makishima–Mackenzie model for  $\text{SiO}_2$ – $\text{Na}_2\text{O}$ – $\text{CaO}$  glasses doped with  $\text{Sb}_2\text{O}_3$  contents. The calculated elastic moduli (Young's, bulk, shear, and longitudinal modulus) were observed to increase with an increase in the  $\text{Sb}_2\text{O}_3$  contents. The microhardness showed an increase, while Poisson's ratio decreased with the rise of the  $\text{Sb}_2\text{O}_3$  contents. In addition, gamma-ray and neutron shielding parameters were evaluated for the investigated glasses. The linear attenuation coefficient (LAC) was simulated using the Monte Carlo N-particle transport code (MCNP-5). Other parameters, such as the mass attenuation coefficient (MAC), transmission factor (TF), and half-value layer, were calculated based on the simulated LAC. The addition of  $\text{Sb}_2\text{O}_3$  content was observed to enhance the investigated glasses' shielding parameters, where the highest LAC was achieved for the SCNSb10 glass with 10 mol%  $\text{Sb}_2\text{O}_3$  and decreased from 0.441 to 0.154  $\text{cm}^{-1}$  at gamma energies between 0.248 and 1.406 MeV. Furthermore, the fast neutron effective removal cross-section ( $\Sigma_R$ ) was computed theoretically. The calculated results showed that the highest  $\Sigma_R$  was equal to 0.0341  $\text{cm}^2\text{g}^{-1}$  and was obtained for the SCNSb0 glass, which had no  $\text{Sb}_2\text{O}_3$  content, while the lowest  $\Sigma_R$  was equal to 0.0286  $\text{cm}^2\text{g}^{-1}$  for the SCNSb10 glass sample. The present work was carried out to examine the advantages of the soda–lime glasses with different  $\text{Sb}_2\text{O}_3$  contents in several photon shielding applications, especially for radiation safety in nuclear installations.

**Keywords:** glass-based hybrid material; mechanical properties; softening temperature; gamma-ray shielding features; Monte Carlo simulation



**Citation:** Sayyed, M.I.; Mahmoud, K.A.; Tashlykov, O.L.; Khandaker, M.U.; Faruque, M.R.I. Enhancement of the Shielding Capability of Soda–Lime Glasses with  $\text{Sb}_2\text{O}_3$  Dopant: A Potential Material for Radiation Safety in Nuclear Installations. *Appl. Sci.* **2021**, *11*, 326. <https://doi.org/10.3390/app11010326>

Received: 31 October 2020

Accepted: 14 December 2020

Published: 31 December 2020

**Publisher's Note:** MDPI stays neutral with regard to jurisdictional claims in published maps and institutional affiliations.



**Copyright:** © 2020 by the authors. Licensee MDPI, Basel, Switzerland. This article is an open access article distributed under the terms and conditions of the Creative Commons Attribution (CC BY) license (<https://creativecommons.org/licenses/by/4.0/>).

## 1. Introduction

Various glass-based systems have their own medical, industrial, and technological applications due to their intrinsic magnetic, optical, physical, structural, and mechanical features. These properties, in principle, can be measured in house-based laboratories due to their ease of modification and access for certain experimental setups [1–4]. On the other hand, radiation–matter interactions may be best performed at synchrotron-based facilities such as the Deutsches Elektronen-Synchrotron (DESY) (Hamburg, Germany), European Synchrotron Radiation Facility (ESRF) (Grenoble, France), or National Synchrotron Light Source (NSLS) (Brookhaven, NY, USA). Unfortunately, access to these worldwide state-of-art laboratories is very restricted for users due to their tight beam time schedule.

Therefore, theoretical calculations or numerical simulations may be used as one alternative to overcome these experimental deficiencies in order to shed light on X-ray or  $\gamma$ -ray radiation–matter interactions. For this purpose, the study will focus on calculations and simulations of  $\text{SiO}_2$ – $\text{Na}_2\text{O}$ – $\text{CaO}$  glasses with different contents of  $\text{Sb}_2\text{O}_3$  (see below), which have emerged in different applications [5]. Heavy metal oxide (HMO) glasses, such as  $\text{Bi}_2\text{O}_3$ ,  $\text{Sb}_2\text{O}_3$ , and  $\text{PbO}$ , have been investigated due to their interesting properties in infrared and nonlinear optics [6]. Additionally, soda–lime–silica glasses are currently the subject of extensive research because of their various applications in medical and dental fields, in addition to their utilization in industrial applications [7,8]. Moreover, soda–lime–silica glasses have been utilized as radiation-sensitive dosimeters and are desirable glasses for the preparation of cheap integrated optical amplifiers [9].

However, some studies have exemplified the different types of glass systems for their potential use as shielding materials. Singh et al. [10] estimated several attenuation parameters of barium borate–flyash glass samples at different photon energies using an experimental setup. The authors reported that these samples are better photon shields in comparison to some types of concretes. Manohara et al. [11] evaluated the effective atomic number and other relevant quantities for borate glasses with  $\text{Bi}_2\text{O}_3$ ,  $\text{PbO}$ ,  $\text{CaO}$ , and  $\text{SrO}$ , using photon interaction cross-sections. They found that the glass samples with both  $\text{PbO}$  and  $\text{Bi}_2\text{O}_3$  were promising photon shielding mediums due to the high  $Z_{\text{eff}}$  of these HMOs, which leads to a high absorption of photons. They also concluded that  $\text{Bi}_2\text{O}_3$  is an excellent alternative to  $\text{PbO}$  for radiological protection. Kurtulus and Kavaz [12] have investigated the shielding factors of waste soda–lime–silica glasses with several amounts of  $\text{SrO}$  using a computer program called Phy-X. They found that the glass with 15 wt% of  $\text{SrO}$  had the highest attenuation factors (both mass and linear) and the lowest half-value thickness. Sallam et al. [13] fabricated bismuth borate glass samples doped with Ni, Cu, and Co using a traditional melting technique and reported the radiation shielding characteristics using an experimental method at four energies (between 662 and 1333 keV). They found that the addition of 0.7% of Ni, Cu, and Co to the bismuth borate glasses enhanced the fabricated samples' shielding ability because these transition metal oxides can have several valance numbers. Al-Hadeethi and Sayyed [14] applied Geant4 simulation to determine the gamma attenuation features for borosilicate systems doped with  $\text{TiO}_2$ ,  $\text{Bi}_2\text{O}_3$ , and  $\text{BaO}$ . They studied the influence of each of these three heavy metal oxides on the half-value layer of the samples at 0.347 and 1.275 MeV. They also compared the radiation shielding parameters for the undoped glass with the glasses doped with  $\text{TiO}_2$ ,  $\text{Bi}_2\text{O}_3$ , and  $\text{BaO}$  to understand the effect of these oxides on the shielding features of the borosilicate glasses. Sayyed and Lakshminarayana [15] fabricated five glass samples containing a fixed content of  $\text{TeO}_2$  (5 mol%) and different amounts of  $\text{BaO}$  (5 to 25 mol%), and studied the physical and attenuation characteristics of these glasses using several techniques. They concluded that the glass with 25 mol% of  $\text{BaO}$  has a thinner half-value layer than the other samples.

All of the aforementioned studies indicated that the inclusion of heavy metal oxides such as  $\text{PbO}$ ,  $\text{BaO}$ ,  $\text{Bi}_2\text{O}_3$  and  $\text{Sb}_2\text{O}_3$  may help to enhance the shielding capability of the glass system. In fact, adding  $\text{Sb}_2\text{O}_3$  to the glasses leads to the enhancement of the physical properties such as the density, refractive index, thermal and mechanical durability etc. [16]. Additionally, glasses with  $\text{Sb}_2\text{O}_3$  exhibit novel optical properties with high transparency to infrared radiation making them potential candidate materials for non-linear optical devices. Moreover, the addition of  $\text{Sb}_2\text{O}_3$  to the glasses may cause glasses to be more resistant to the formation of high energy radiation-induced defects [5]. Furthermore, the addition of  $\text{Sb}_2\text{O}_3$  has an important role to enhance the attenuation performance of the glasses against ionizing radiation [5]. In the current work, the effects of antimony on the radiation shielding and mechanical features of soda–lime–silica glasses were investigated. The mass/linear attenuation parameters, transmission factor, dose rate, and the half-value layer of all compounds were evaluated to evaluate the glasses' radiation shielding efficiency.

These properties reveal the interactions between  $\gamma$ -rays and these glasses for uses in medical and industrial applications. All of the previously reported studies evaluating some

systems' shielding features have been carried out either experimentally or theoretically based on XCOM software. However, there are a limited number of studies in the literature that have used the MCNP-5 code to investigate the shielding characteristics of glass samples [7–19]. This comprehensive study may stimulate scientists working in synchrotron-based facilities to perform experimental studies on these compounds to compare these results with their future experimental data on these samples. This theoretical study may also help people working in industrial and medical applications to design new related compounds for tunable radiation resistance devices.

In this work, the mechanical and shielding features for soda–lime–silica glasses were reported. The effects of  $\text{Sb}_2\text{O}_3$  on the mechanical and shielding parameters of the selected soda–lime–silica glasses were also investigated.

## 2. Materials and Methods

### 2.1. Mechanical Properties Calculations Using Makishima–Mackenzie Model

The Makishima–Mackenzie model was applied to predict the elastic properties of the  $\text{SiO}_2$ – $\text{Na}_2\text{O}$ – $\text{MgO}$ – $\text{CaO}$ – $\text{Al}_2\text{O}_3$  glasses doped with  $\text{Sb}_2\text{O}_3$  content. The present glass samples were collected from reference [5]. The composition, density, molecular weight, and molecular volume of the studied samples are presented in Table 1.

**Table 1.** The chemical composition, density molecular weight, and molar volume of the investigated glasses.

Glass Code	Chemical Composition (wt%)						Density (g/cm <sup>3</sup> )	Molecular Weight (g/mol)	Molar Volume (cm <sup>3</sup> /mol)
	$\text{Al}_2\text{O}_3$	$\text{CaO}$	$\text{MgO}$	$\text{Na}_2\text{O}$	$\text{Si}_2\text{O}$	$\text{Sb}_2\text{O}_3$			
SCBSb0	1.305	9.410	2.675	14.002	72.608	0.000	2.499	59.358	23.753
SCBSb0.5	1.630	9.124	2.558	13.671	70.662	2.355	2.537	60.661	23.911
SCBSb1	1.943	8.829	2.506	13.202	68.813	4.708	2.603	61.924	23.790
SCBSb5	9.516	6.667	1.827	10.060	51.309	20.621	2.839	74.360	26.192
SCBSb10	13.364	4.807	1.337	7.592	38.243	34.657	3.002	88.657	29.509

The elastic moduli were theoretically predicted for the silicate glasses using Makishima–Mackenzie's model [20,21]. The Makishima–Mackenzie model reports that Young's modulus depends on the values of dissociation energy ( $G_t$ ) and the packing density ( $V_t$ ) of the metal oxides constituting the glass network:

$$G_t \left( \text{kJ cm}^{-3} \right) = \sum_i X_i G_i \quad (1)$$

where  $X_i$  and  $G_i$  refer to the molar fraction and the dissociation energy of the  $i$ th constituting compound. The  $G_i$  is related to the standard heat of formation ( $\Delta H_f$ ) for each compound and determined from Equation (2).

$$G_i \left( \text{kJ cm}^{-3} \right) = \frac{\rho_i}{M_i} \left( X \Delta H_f(\text{metal}) + Y \Delta H_f(\text{oxygen}) - \Delta H_f(\text{compound}) - (X + Y)RT \right) \quad (2)$$

where  $\rho_i$ ,  $M_i$ ,  $\Delta H_f(\text{metal})$ ,  $\Delta H_f(\text{oxygen})$ ,  $\Delta H_f(\text{compound})$ ,  $X$ , and  $Y$  are the density of compound, molar weight of the compound, enthalpy of metal, enthalpy of oxygen, enthalpy of compound, the number of atoms of metal and oxygen, respectively, at the room temperature.

$$V_t \left( \text{cm}^3 \text{ mol}^{-1} \right) = \frac{\rho}{M} \sum_i X_i V_i \quad (3)$$

where  $V_i$  represents the packing factor of the  $i$ th constituent compound in the glass network.

Based on the values of  $G_t$  and  $V_t$ , the elastic properties (Young's modulus ( $Y$ ), bulk modulus ( $B$ ), shear modulus ( $S$ ), longitudinal modulus ( $L$ ), Poisson's ratio ( $\mu$ ), micro-hardness ( $H$ ), and softening temperature ( $T_g$ )) can be evaluated through the following formulas.

$$Y = 2V_t G \quad (4)$$

$$B = 1.2 V_t E \quad (5)$$

$$S = \frac{3 Y B}{(9B - Y)} \quad (6)$$

$$L = B + \frac{3}{4} S \quad (7)$$

$$\mu = \frac{Y}{2 S} - 1 \quad (8)$$

$$H = \frac{(1 - 2\mu)}{6(1 + \mu)} \quad (9)$$

$$T_g = \frac{M}{0.5074 \rho v_s^2} \quad (10)$$

## 2.2. Radiation Shielding Properties Using MCNP-5 Code

Monte Carlo code with continuous-energy nuclear and atomic data libraries was applied to simulate the studied samples' radiation shielding properties. The MCNP nuclear database's main sources are ENDF, ACTI, ENDL, ACTI, and T-16 files [22]. An input file was formatted to estimate the simulated average track lengths of the incoming photons in the studied glasses. This input file contained all the information about the glass samples (density, chemical composition, and dimensions), detector, source, and geometry. The geometry used in the present study is described in Figure 1, where the studied samples were placed between the radioisotopes and the F4 tally detector [23–25]. In the present study, various sources such as Th-228 ( $E = 0.24$  MeV), Rn-222 ( $E = 0.51$  MeV), Cs-137 ( $E = 0.66$  MeV), Co-60 ( $E = 1.17$  and  $1.33$  MeV), and Eu-152 ( $E = 1.40$  MeV) were used. Photons emitted from the source were collimated using a lead collimator.

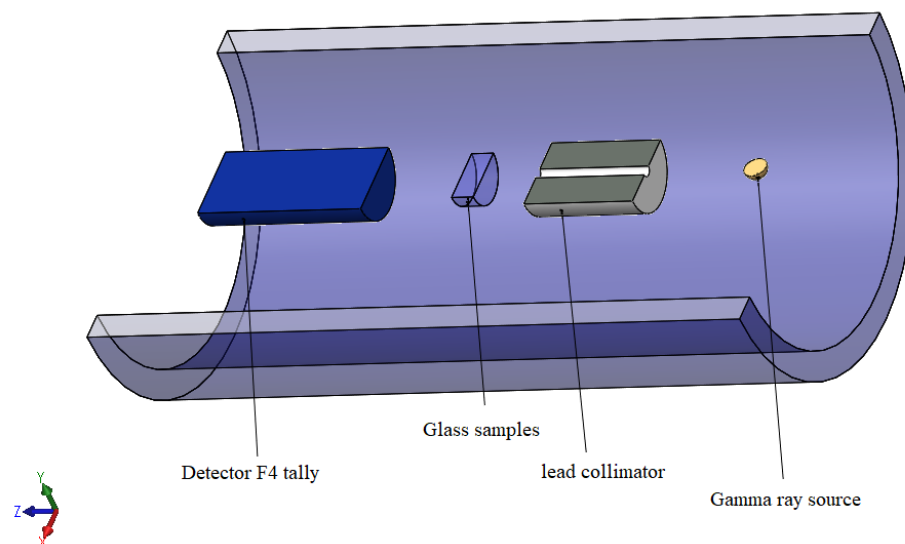


**Figure 1.** The simulation geometry setting.

After that, the shielding parameters such as linear and mass attenuation coefficients (LAC/MAC), half-value layer (HVL), transmission factor (TF), dose rate, and radiation protection efficiency (RPE) were determined using the simulated data with the help of the following equations.

$$LAC \left( \text{cm}^{-1} \right) = \frac{1}{x} \ln \left( \frac{I_0}{I} \right) \quad (11)$$

$$\mu_m = \frac{LAC \left( \text{cm}^{-1} \right)}{\rho \left( \text{g cm}^{-3} \right)} \quad (12)$$

$$TF = \frac{I}{I_0} = \exp(-LAC * x) \quad (13)$$

$$HVL = \frac{\ln(2)}{LAC \text{ (cm}^{-1}\text{)}} \quad (14)$$

$$MFP = \frac{1}{LAC \text{ (cm}^{-1}\text{)}} \quad (15)$$

where  $I_0/I$ ,  $x$ ,  $\rho$  and  $w_i$ , represent the incoming/transmitted photon intensities, glass thickness, glass density and fractional weight of the  $i$ th constituent element, respectively.

Equations (16) and (17) were utilized to theoretically calculate the fast neutron significant removal cross-section  $\sum_R$  ( $\text{cm}^2\text{g}^{-1}$ ) using the atomic number of the constituent metal oxides [26].

$$\sum_R = 0.190 Z^{-0.743} \quad (Z \leq 8) \quad (16)$$

$$\sum_R = 0.125 Z^{-0.565} \quad (Z > 8) \quad (17)$$

### 3. Results and Discussion

#### 3.1. Mechanical Properties

The elastic moduli (Young's, bulk, shear, and longitudinal), Poisson's ratio ( $\mu$ ), micro-hardness ( $H$ ), and softening temperature were evaluated theoretically at room temperature (298 K) based on the Makishima–Mackenzie theory. According to this theory, the packing factor ( $V_i$ ) and dissociation energy per unit volume ( $G_t$ ,  $\text{kJ}/\text{cm}^3$ ) are the essential parameters used to predict glassy systems' mechanical properties. The calculated data of  $G_t$ ,  $V_i$ , and packing density ( $V_t$ ) are summarized in Table 2. Figure 2 illustrated the calculated values of  $G_t$  and packing density ( $\text{cm}^3/\text{mol}$ ) of the studied SCNSb samples. The results revealed that the behavior of the calculated dissociation energy ( $G_t$ ,  $\text{kJ}/\text{cm}^3$ ) with the  $\text{Sb}_2\text{O}_3$  content is opposite to that of the packing density ( $V_t$ ). The calculated values of dissociation energy for the SCNSb samples increased gradually from 63.980 to 68.297  $\text{kJ}/\text{cm}^3$ , while the  $V_t$  decreased from 0.545 to 0.538  $\text{cm}^3/\text{mol}$ , raising the  $\text{Sb}_2\text{O}_3$  content from 0 to 10 mol % and  $\text{Al}_2\text{O}_3$  from 0.76 to 11.72 mol %. The sudden increase in the  $G_t$  is due to the high rise in the  $\text{Sb}_2\text{O}_3$  and  $\text{Al}_2\text{O}_3$  contents in the last two samples, SCNSb 5 and SCNSb 10. The  $\text{Al}_2\text{O}_3$  jumped from 1.18 mol % (for SCNSb 1) to 6.94 mol % (for SCBSb 5), and then 11.72 mol % (for SCNSb 10). Moreover, the  $\text{Sb}_2\text{O}_3$  contents jumped from 1 mol % (for SCNSb 1), to 5.26 mol % (for SCNSb 5), and then to 10.54 mol % (for SCNSb 10).

Table 2. The mechanical properties of the investigated glasses.

Glass Code	The Mechanical Properties									Softening Temperature ( $^{\circ}\text{C}$ )
	$V_i$ ( $\text{cm}^3/\text{mol}$ )	$G$ ( $\text{kJ}/\text{cm}^3$ )	$V_t$	$E$ (GPa)	$B$ (GPa)	$S$ (GPa)	$\mu$	$H$ (GPa)	$L$ (GPa)	
SCBSb0	12.939	63.980	0.545	69.707	45.568	27.994	0.2450	4.758	82.893	524.395
SCBSb0.5	13.023	64.015	0.545	69.732	45.576	28.005	0.2450	4.761	82.915	520.176
SCBSb1	13.093	64.047	0.544	70.498	46.560	28.253	0.2446	4.753	84.230	512.424
SCBSb5	13.996	66.678	0.542	72.264	46.991	29.052	0.2437	4.964	85.727	508.887
SCBSb10	14.919	68.297	0.538	73.553	47.528	29.609	0.2421	5.091	87.007	506.031

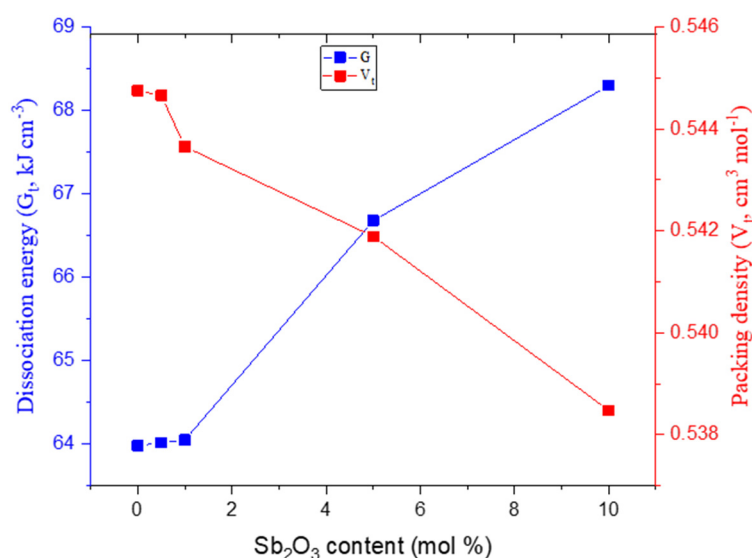


**Figure 2.** Variation of the dissociation energy per unit volume and the packing density of the studied glasses as a function of Sb<sub>2</sub>O<sub>3</sub> contents.

The increase in  $G_t$  is also related to the replacement of the SiO<sub>2</sub> ( $G_i = 68$  kJ/cm<sup>3</sup> and  $V_i = 14$  cm<sup>3</sup>/mol), CaO ( $G_i = 64.1$  kJ/cm<sup>3</sup> and  $V_i = 9.4$  cm<sup>3</sup>/mol), Na<sub>2</sub>O ( $G_i = 31.9$  kJ/cm<sup>3</sup> and  $V_i = 11.2$  cm<sup>3</sup>/mol), and MgO ( $G_i = 90$  kJ/cm<sup>3</sup> and  $V_i = 7.6$  cm<sup>3</sup>/mol) by Sb<sub>2</sub>O<sub>3</sub> ( $G_i = 35.3$  kJ/cm<sup>3</sup> and  $V_i = 23$  cm<sup>3</sup>/mol) [27], and Al<sub>2</sub>O<sub>3</sub> ( $G_i = 131$  kJ/cm<sup>3</sup> and  $V_i = 21$  cm<sup>3</sup>/mol). The mentioned values of the dissociation energy are related to the standard heat of formation (enthalpy) for each constituting compound, which is described by Equation (2).

The theoretical results of elastic moduli (Young's, bulk, shear, and longitudinal) are also listed in Table 2. As mentioned in Equations (3)–(6), the elastic moduli are directly proportional to  $V_t$  and  $G_t$ . In the present study, this is true for dissociation energy, where the elastic moduli are directly proportional to the  $G_t$ , while being inversely proportional to the packing factor  $V_i$  for all the studied glasses. Figure 3 depicts the variation of elastic moduli against the Sb<sub>2</sub>O<sub>3</sub> contents. The estimated values of elastic moduli demonstrated a strong dependence on the oxides' composition in the SCNSb glass network. Young's, bulk, shear, and longitudinal moduli increase proportionally with the Sb<sub>2</sub>O<sub>3</sub> content. The straight red lines in Figure 3 represent the linear fitting of the calculated results, where the values of R-squared are 0.962, 0.812, 0.971, and 0.920 for  $Y$ ,  $B$ ,  $S$ , and  $L$  moduli, respectively.

As mentioned in Equation (8), Poisson's ratio is directly proportional to Young's modulus. Thus, Figure 4 depicts that Poisson's ratio ( $\mu$ ) for the chosen samples decreases with an increase in the Sb<sub>2</sub>O<sub>3</sub> content. The calculated results showed that Poisson's ratio reduced from 0.2450 to 0.2421 as the content of Sb<sub>2</sub>O<sub>3</sub> changed from 0 to 10 mol%. In comparison, the micro-hardness increases gradually with an increase in the Sb<sub>2</sub>O<sub>3</sub> content. It is increased from 4.758 to 5.091 GPa with an increase in the Sb<sub>2</sub>O<sub>3</sub> content between 0 and 10 mol%. The reason for this increase is the inverse proportionality between the micro-hardness and Poisson's ratio (see Equation (9)).

The softening temperature ( $T_g$ ) is a critical temperature in which the glass transition takes place. The  $T_g$  for the studied SCNSb samples is shown in Figure 5. The calculated values of  $T_g$  decreased gradually with the insertion of Sb<sub>2</sub>O<sub>3</sub> content. The  $T_g$  values decreased from 524.39 to 506.031 °C. This was due to the replacement of SiO<sub>2</sub>, which has a high melting temperature ( $T = 1710$  °C), with Sb<sub>2</sub>O<sub>3</sub>, which has a lower melting temperature ( $T = 656$  °C). The obtained results agreed with reference [28] reported by Bloomfield. Bloomfield concluded that for alkaline-based silicate glasses, the oxygen and metal atoms in the alkaline structure are held together by ionic bonds rather than covalent bonds. The metal atoms lose electrons while the oxygen atom takes these electrons.



Thus, a mixture of positively charged metal ions and negatively charged oxygen ions are produced. After that, the oxygen atom binds with one silicon atom, and no bridge is formed between pairs of silicon atoms. Hence, the melting temperature and softening temperature decreased considerably.

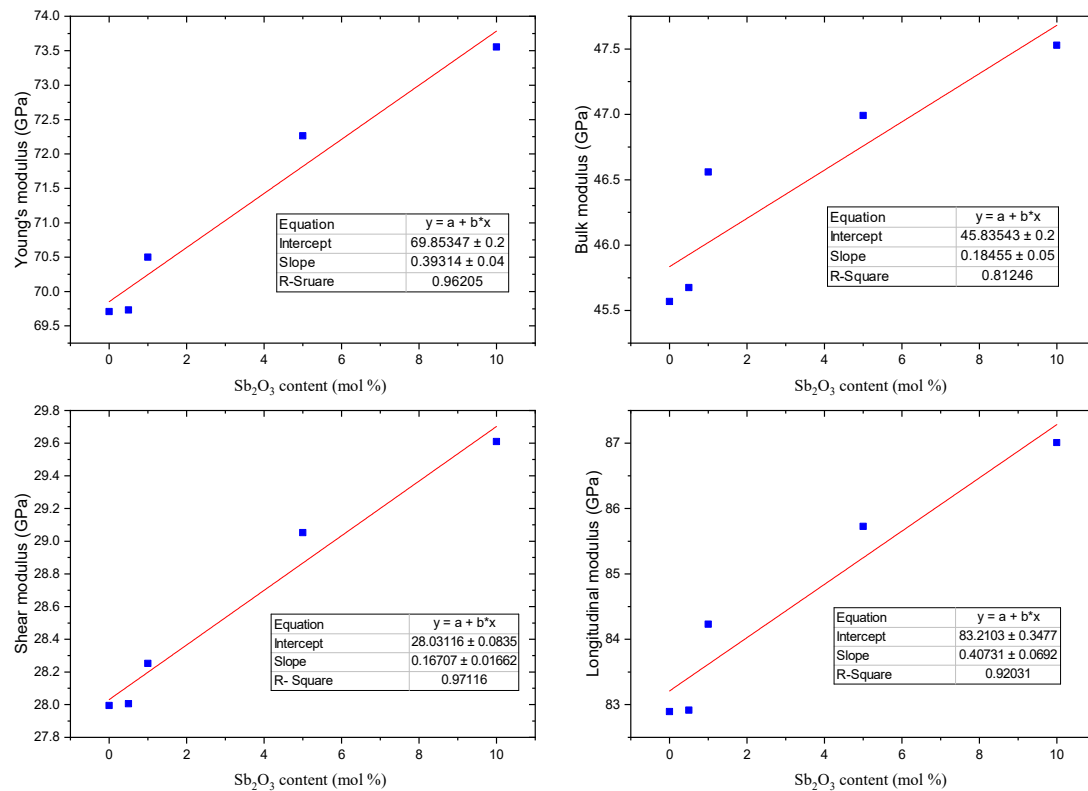


**Figure 3.** The variation of elastic moduli versus the  $\text{Sb}_2\text{O}_3$  content.

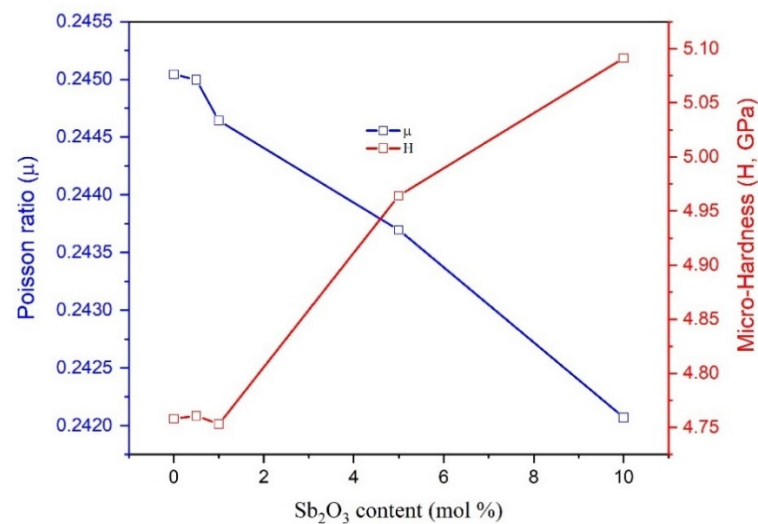


**Figure 4.** Variation of Poisson's ratio and micro-hardness of the studied glasses as a function of the  $\text{Sb}_2\text{O}_3$  contents.

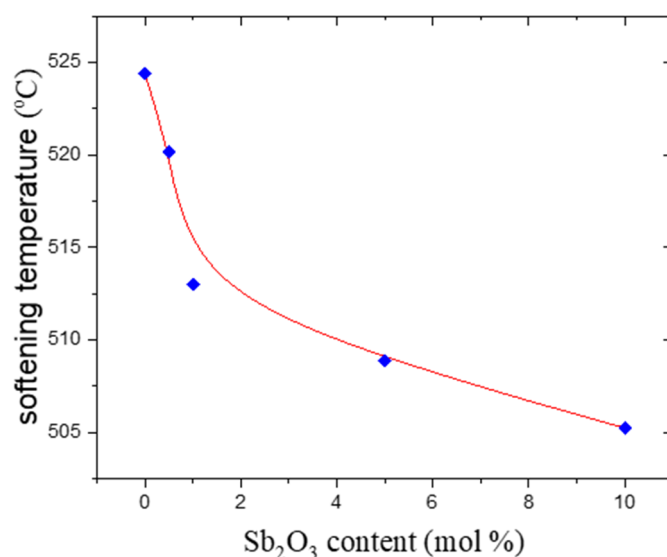


**Figure 5.** Dependence of the softening temperature on the Sb<sub>2</sub>O<sub>3</sub> contents.

### 3.2. Radiation Shielding Attributes

The LAC was simulated using MCNP-5 and plotted in Figure 6. The simulated LAC values are affected by two significant parameters. The incoming gamma photon energy is the first. The simulated values of LAC decreased when the incoming radiation energy increased. The LAC's highest values were recorded for gamma energy of 0.248 MeV and varied in the range between 0.288–0.441 cm<sup>−1</sup> for glasses BCNSb0 and BCNSb10, respectively. Furthermore, an increase in the incoming photon energy resulted in a more significant decrease in LAC values. This decrease is related to the interaction type of gamma photons with the glass atoms. In the studied energy zone (0.248–1.406 MeV), Compton scattering interactions (CS) are predominant, and the CS cross-section is opposite to the incoming photon energy ( $\sigma_{com} \propto \frac{1}{E}$ ) [29]. Around 1.406 MeV, the LAC's lowest values were recorded, and they varied in the range between 0.132–0.154 cm<sup>−1</sup> for glasses SCNSb0 and SCNSb10, respectively.

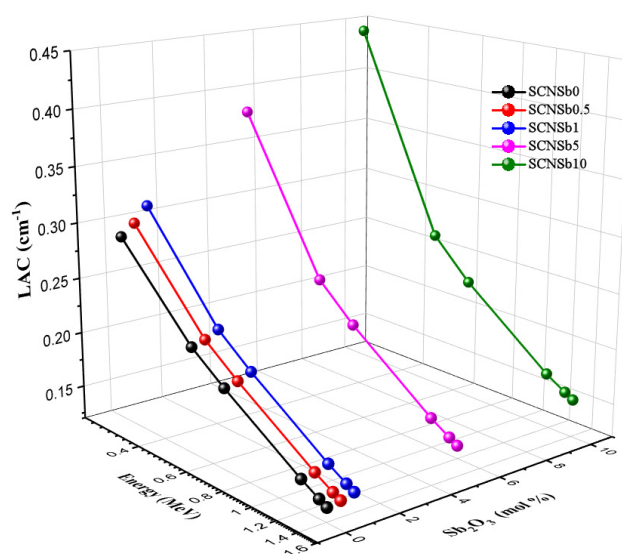


**Figure 6.** Variation of the linear attenuation coefficient LAC of the studied glasses versus the gamma photon energies and Sb<sub>2</sub>O<sub>3</sub> contents.



The chemical composition of the studied glasses ( $\text{Sb}_2\text{O}_3$  insertion) represents the second factor that affects the LAC values. As mentioned in Figure 6, the replacement of the  $\text{SiO}_2$  by  $\text{Sb}_2\text{O}_3$  increases the studied glasses' simulated LAC. This trend is related to  $\text{SiO}_2$  having a lower density and molecular weight ( $\rho = 2.65 \text{ g cm}^{-3}$  and  $\text{MW} = 60.08 \text{ g mol}^{-1}$ ) being replaced by  $\text{Sb}_2\text{O}_3$  (for this oxide,  $\rho = 5.2 \text{ g cm}^{-3}$  and  $\text{MW} = 291.52 \text{ g mol}^{-1}$ ). The greatest LAC was achieved for SCNSb10 glass with 10 mol %  $\text{Sb}_2\text{O}_3$  content and varied in the range between  $0.154\text{--}0.441 \text{ cm}^{-1}$ , while the lower LAC obtained for glass SCNSb0 without  $\text{Sb}_2\text{O}_3$  and changed between  $0.132\text{--}0.288 \text{ cm}^{-1}$  at gamma photon energies between  $0.248\text{--}1.406 \text{ MeV}$ , respectively. The recorded increase is related to CS interactions, where the CS cross-section linearly increases with an increase in the  $Z_{\text{eff}}$  of the studied samples ( $\sigma_{\text{com}} \propto Z_{\text{eff}}$ ).

The MAC was determined from the simulated LAC, according to Equation (11). It was also calculated theoretically using the XCOM program reported by Bereg and Hubell [30]. Figure 7 showed that the MAC has a trend line similar to the one discussed earlier regarding the LAC and is also affected by the incoming gamma photon energy and the glass chemical composition. The highest MAC was achieved at lower energies ( $0.248 \text{ MeV}$ ) and varied in the range between  $0.115\text{--}0.147 \text{ cm}^2/\text{g}$ , but the smallest MAC was found at higher energies ( $1.406 \text{ MeV}$ ) and ranged between  $0.0531\text{--}0.0513 \text{ cm}^2/\text{g}$  for the studied SCNSb0 and SCNSb10 glasses, respectively. Figure 8 showed that the simulated and theoretical MAC are close together, with the correlation coefficient (R-squared) being equal to 0.999 for SCNSb10 as an example. This reflected the accuracy of the simulation process.

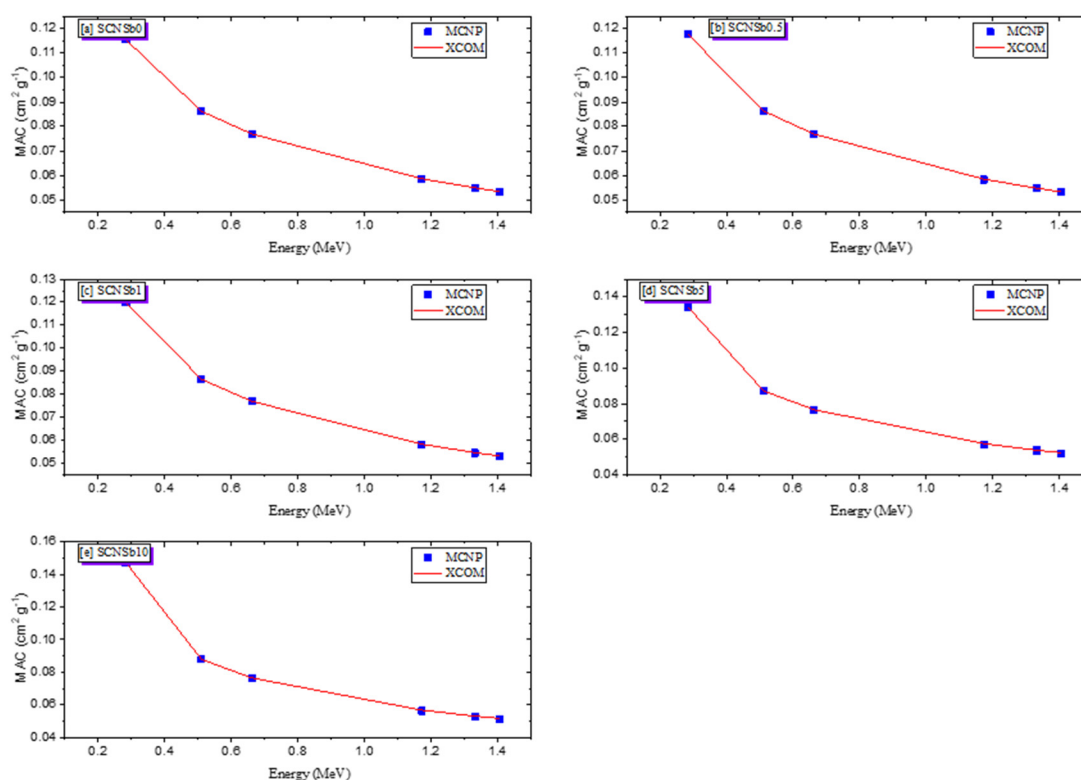
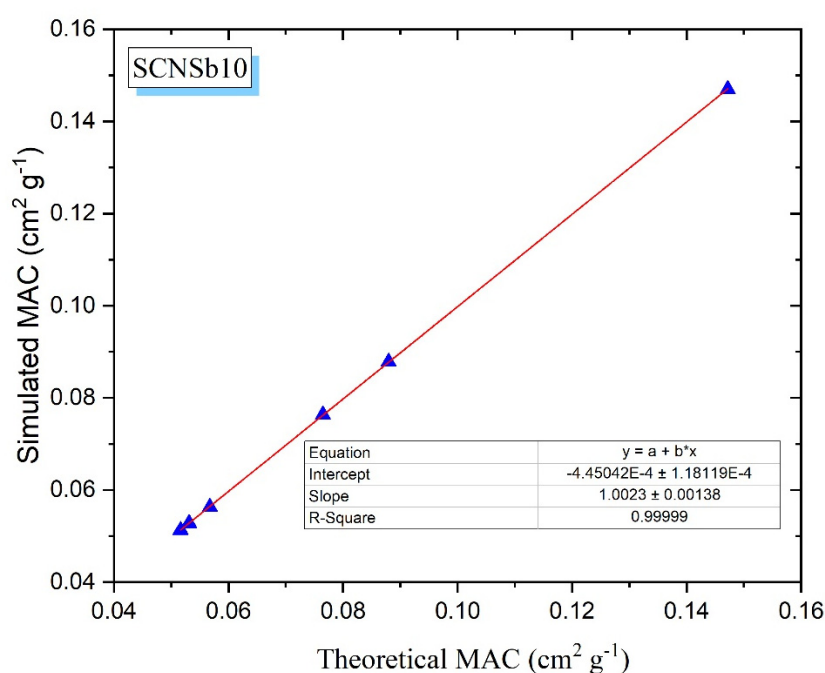


Figure 7. Comparison between the simulated and calculated MAC for the studied glasses.

The transmission factor (TF) is an important parameter that predicts the number of photons that penetrate the investigated sample. The TF changes for all SCNSb0–SCNSb10 glass samples with the glass thickness and incoming photon energies are illustrated in Figure 9. The incoming photon energy represents the TF's main parameter, where the TF values increase linearly with an increase in photon energy. A lower TF was predicted at low energies ( $0.248 \text{ MeV}$ ), which decreased in range  $74.941\text{--}64.314\%$  for glasses SCNSb0 and SCNSb10, respectively, for a thickness of  $1 \text{ cm}$  (as an example). On the other hand,

the highest TF was achieved at higher gamma photon energies (1.406 MeV) and varied in the range of 85.720–87.563% for glasses SCNSb0 and SCNSb10, respectively. The direct proportion between the TF and the incoming energy results from the photon penetration power (PP) that increases with an increase in the incoming photon energy and a decrease in the photon wavelength ( $\lambda$ ) ( $PP \propto \frac{E}{\lambda}$ ). The glass thickness is another factor that has a significant effect on the value of TF. As mentioned in Figure 9, the TF is inversely proportional to the sample thickness. Thus, the biggest TF was reported for thinner glasses, while the lowest TF was achieved for thicker glasses. For the SCNSb10 glass (as an example), the TF decreased from 64.314 to 11.003% when the thickness increased from 1 to 5 cm, respectively, at 0.248 MeV. The inverse relation between the glass thickness and the TF is related to the number of collisions between the photons and the glass atoms in each thickness. The number of collisions for thicker glasses is greater than those of the thinner samples.



**Figure 8.** Correlation between simulated and calculated MAC for glass SCNSb10 as an example.

The HVL predicts the glass material's width needed to minimize the photon intensity to half of its incoming value. As shown in Figure 10, the HVL is affected by the incoming photon energy and the material composition. Figure 10 illustrates a positive correlation between the simulated HVL and the photon energies. As previously mentioned, the straight proportion is due to CS interactions. The thinnest HVL was noticed at 0.248 MeV, while the thickest HVL was achieved at high energy (1.406 MeV). The thinner values of the HVL varied between 1.570–2.402 cm, while the thickest HVL varied between 4.498–5.219 cm for glasses SCNSb10 and SCNSb0, respectively. The material composition also has a remarkable effect on the predicted HVL values. The replacement of  $\text{SiO}_2$  with  $\text{Sb}_2\text{O}_3$  helps to enhance the material density and the electron density of the investigated samples. Thus, the number of gamma photon collisions increases, resulting in more attenuation of the incoming photons. As mentioned in Figure 10, the thinnest HVL was achieved for SCNSb10 glasses with 10 mol %  $\text{Sb}_2\text{O}_3$ , while the thickest HVL was achieved for the SCNSb0 glass without  $\text{Sb}_2\text{O}_3$  content.

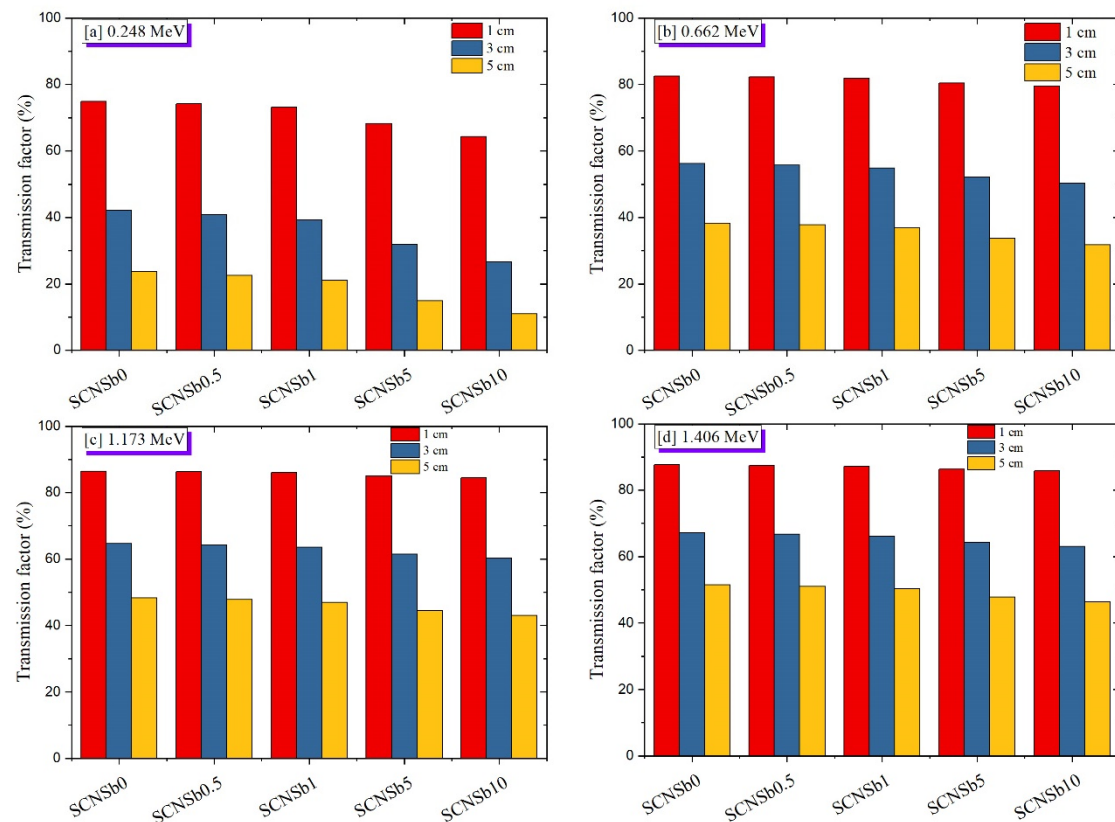


**Figure 9.** Variation of the transmission factor as a function of the glass thickness at some fixed energies: (a) 0.248 MeV, (b) 0.662 MeV, (c) 1.173 MeV, (d) 1.406 MeV.

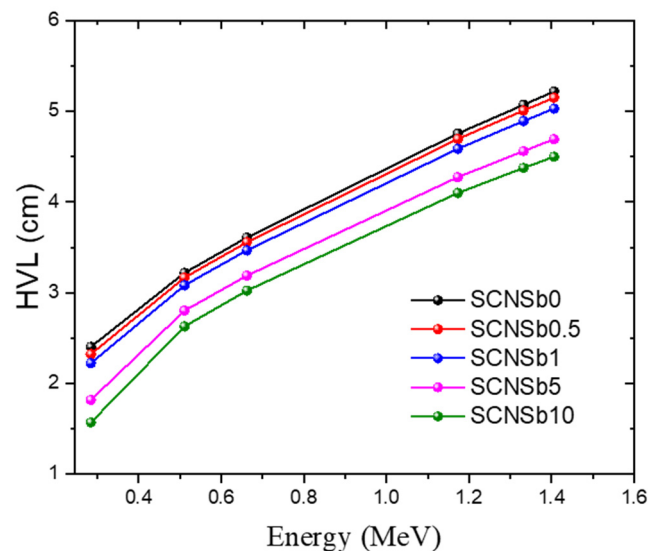


**Figure 10.** Variation of the HVL of the studied glasses as a function of the incoming photon energy.

The mean free path (MFP) is used to predict the average distance between two gamma collisions. We can connect the MFP with the HVL via the relationship ( $MFP = \frac{HVL}{\ln(2)}$ ). Thus, the MFP's estimated values have a similar trend and discussion, as presented in the HVL section (see Figure 11). The smallest distance between two gamma collisions was achieved for the SCNSb10 glass and varied in the range 2.265–6.490 cm, while the most significant distance obtained varied in the range between 3.466–7.529 cm and was achieved for the

SCNSb0 sample. To check the effectiveness of the current glass systems, the MFP of the studied glasses has been compared to a commercial shielding material (RS253-G18) and a previously prepared shielding material (Borax 40) [31]. As illustrated in Figure 11, the highest MFP was achieved for the Borax 40 glass, while the lowest MFP was achieved for SCNSb10 glass samples. The comparison proved that the studied glasses, SCNSb0-SCNSb10, have MFP values lower than that of Borax 40 and the commercial shielding material RS253-G18.

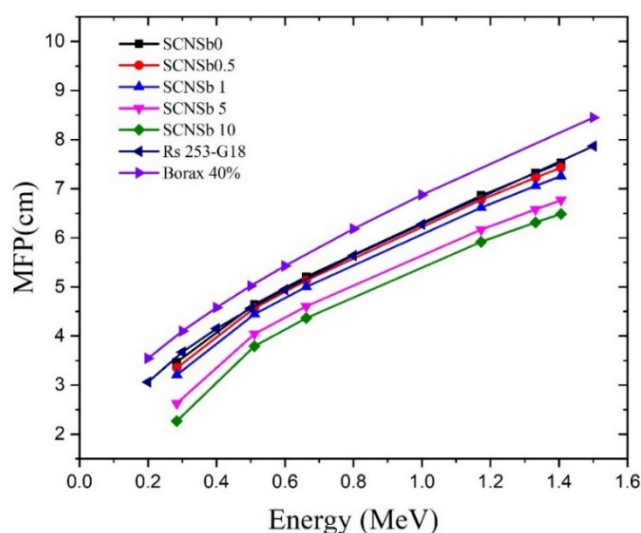


**Figure 11.** Comparison between the mean free path of the studied samples to those of some previously prepared glasses (Borax 40) and standard shielding glass RS 253-G18.

The dose rate received by exposure from a radioactive source without protection is assumed to be 100  $\mu\text{Sv/h}$ . The dose rate received from a shielded radioactive source was calculated and plotted in Figure 12. Two factors appear to affect the dose rate received from the radioactive source. The incoming gamma photon energy is considered as the first factor. The received dose rate is directly proportional to the incoming photon energy. For glasses with a thickness of 5 cm, for example, the dose rate received varied in the range between 23.638–51.476  $\mu\text{Sv/h}$  at gamma energies between 0.248–1.406 MeV. The direct correlation between the dose rate and the incoming energy is related to the photons' penetration power. The penetration power increases with an increase in photon energies. Thus, the incoming photons spend a short time in the glass material. The photons lose a small part of their incoming energies before passing through the shielding material, so the passing photons' dose rate will be high. The glass thickness is the second parameter that affected the received dose rate. The dose rate is exponentially decreased with an increase in the thickness. Figure 12 depicts the high dose rate received from thinner glasses, with the thicker glasses providing better protection.

The SCNSb samples' effectiveness to absorb fast neutrons was studied through the calculation of  $\Sigma_R$  ( $\text{cm}^2/\text{g}$ ) (see Figure 13). It is known that materials doped with light elements and compounds such as C, B, and water ( $\text{H}_2\text{O}$ ) absorb fast neutrons better than those doped with heavy compounds such as  $\text{PbO}$  and  $\text{Sb}_2\text{O}_3$ . In the present work, the glass with a higher ratio of  $\text{Sb}_2\text{O}_3$  possessed a lower fast neutron removal cross-section than the glasses with lower amounts of  $\text{Sb}_2\text{O}_3$ . Thus, the SCNSb10 glass with 10 mol %  $\text{Sb}_2\text{O}_3$  has an  $\Sigma_R = 0.0286 \text{ cm}^2/\text{g}$ , which is lower than the  $\Sigma_R = 0.0341 \text{ cm}^2/\text{g}$  recorded SCNSb0 glass, which has no  $\text{Sb}_2\text{O}_3$  content. The effective removal cross-section affected by the energy of the projected neutrons besides the chemical composition for the studied glass samples. Figure 13 depicts that the  $\Sigma_R$  ( $\text{cm}^2/\text{g}$ ) is exponentially decreased with the increasing of the  $\text{Sb}_2\text{O}_3$  content in the investigated glasses. The partial substitution of the  $\text{SiO}_2$  by  $\text{Sb}_2\text{O}_3$  causes an increase in the effective atomic weight of the investigated glass.

Hence, Equations (16) and (17) showed an inversely relationship between the  $\Sigma_R$  ( $\text{cm}^2/\text{g}$ ) and the  $Z$  of the investigated glass samples, so the  $\Sigma_R$  ( $\text{cm}^2/\text{g}$ ) decreased exponentially with the increasing of the  $Z_{\text{eff}}$ .

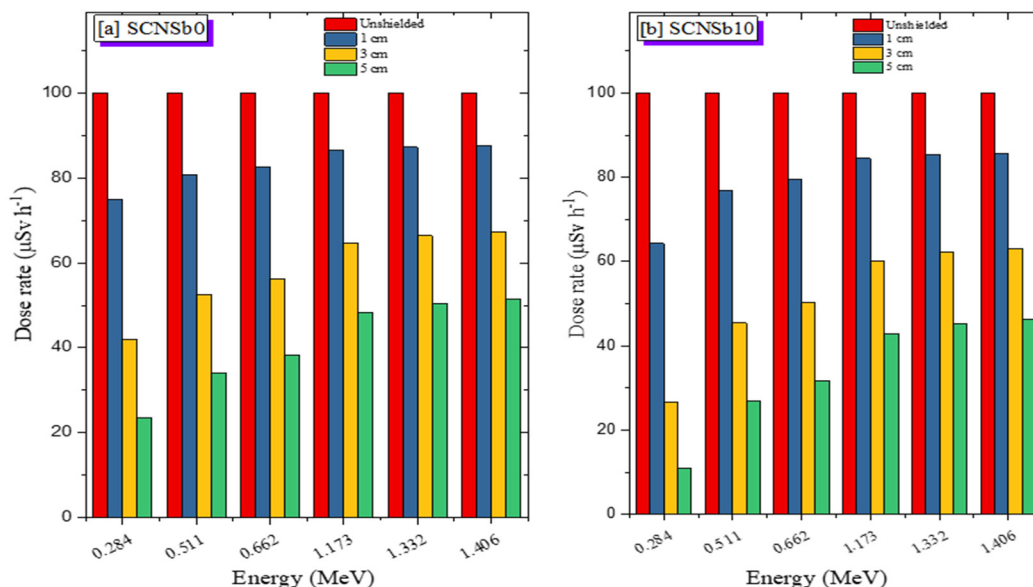


Figure 12. Variation of the dose rate versus the glass thickness for some glass samples: (a) SCNSb0, (b) SCNSb10.

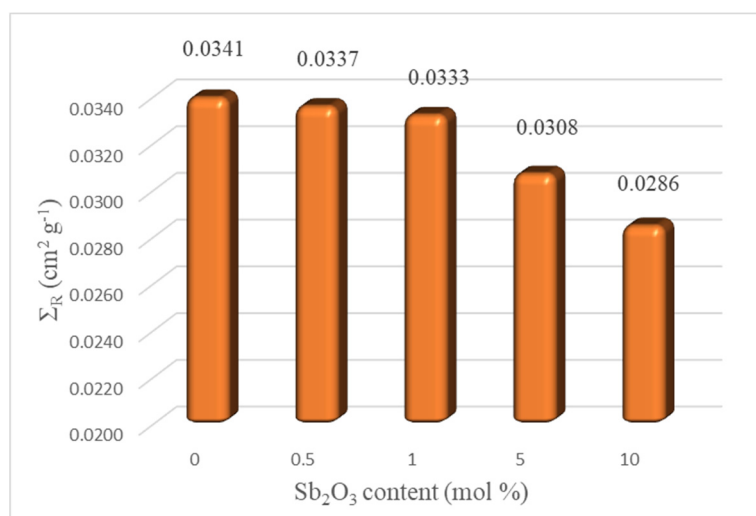


Figure 13. Variation of the effective removal cross-section as a function of the  $\text{Sb}_2\text{O}_3$  contents.

#### 4. Conclusions

The elastic moduli and radiation shielding ability for five soda–lime–silica glasses doped with  $\text{Sb}_2\text{O}_3$  were evaluated. The elastic moduli were calculated using the Makishima–Mackenzie model, and the obtained results depicted that Young's modulus enhanced from 69.707 to 73.553 GPa with an increase in the  $\text{Sb}_2\text{O}_3$  ratio between 0–10 mol %. The bulk, shear, and longitudinal moduli were observed to have the same variation trend with the  $\text{Sb}_2\text{O}_3$  consent as Young's modulus. The micro-hardness was observed to increase from 4.7558 GPa to 5.091 GPa, while Poisson's ratio was reduced from 0.245 to 0.242 for the investigated glasses. Thus, a partial replacement of  $\text{SiO}_2$  with  $\text{Sb}_2\text{O}_3$  and/or the  $\text{Sb}_2\text{O}_3$  dopant enhanced the mechanical features of the soda–lime–silica glasses. MCNP-5 code was utilized to evaluate the gamma-ray shielding features between 0.248–0.1406 MeV. The

simulated linear attenuation coefficient had the highest values for SCNSb10 glasses and varied in the range between  $0.154\text{--}0.441\text{ cm}^{-1}$ , while the lowest values varied between  $0.132\text{--}0.288\text{ cm}^{-1}$  for the SCNSb0 glasses. Other shielding properties such as the mass attenuation coefficient, half-value layer, mean free path, transmission factor, and dose rate were calculated based on the simulated linear attenuation coefficient. Finally, the effective removal cross-section ( $\Sigma_R$ ) was theoretically estimated based on the atomic number of the glass system compounds. The  $\Sigma_R$  varied in the range between  $0.0284\text{--}0.0341$  for glasses SCNSb10 and SCNSb0. This study reveals that the radiation shielding efficiency of soda–lime glass increases with increasing the  $\text{Sb}_2\text{O}_3$  content. Experimental investigation is surely an important task to obtain the real information of radiation interaction parameters. However, such a task may not be always possible due to some limitations. This work contained only simulation results, and it is expected that the present results will assist further experiments in the comparison of the measured data and obtain a clear understanding on radiation–material interactions and associated phenomena.

**Author Contributions:** Conceptualization, M.I.S.; methodology, M.I.S.; software, K.A.M.; validation, K.A.M. and O.L.T.; formal analysis, M.I.S.; investigation, K.A.M.; resources, M.I.S.; data curation, M.I.S.; writing—original draft preparation, K.A.M.; writing—review and editing, M.U.K.; visualization, O.L.T.; supervision, M.U.K.; project administration, M.R.I.F.; funding acquisition, M.R.I.F. All authors have read and agreed to the published version of the manuscript.

**Funding:** This work was funded by the Research Universiti Grant, Universiti Kebangsaan Malaysia, Geran Universiti Penyelidikan (GUP), code: 2018-133, and the APC was funded by code: 2018-133.

**Acknowledgments:** This work was supported by the Research Universiti Grant, Universiti Kebangsaan Malaysia, Geran Universiti Penyelidikan (GUP), code: 2018-133.

**Conflicts of Interest:** The authors declare no conflict of interest.

## References

1. Petr, K.; Ladislav, K.; Petr, M.; Lionel, M.; Bertrand, R. Glass-forming ability and the structure of glasses in the  $\text{BaO}\text{--}\text{WO}_3\text{--}\text{P}_2\text{O}_5$  system. *J. Non-Cryst. Solids* **2020**, *541*, 120145.
2. Khodadadi, A.; Taherian, R. Investigation on the radiation shielding properties of lead silicate glasses modified by ZnO and BaO. *Mater. Chem. Phys.* **2020**, *251*, 123136. [\[CrossRef\]](#)
3. Sayyed, M.; Mohammed, F.Q.; Mahmoud, K.; Lacomme, E.; Kaky, K.M.; Khandaker, M.U.; Faruque, M.R.I. Evaluation of Radiation Shielding Features of Co and Ni-Based Superalloys Using MCNP-5 Code: Potential Use in Nuclear Safety. *Appl. Sci.* **2020**, *10*, 7680. [\[CrossRef\]](#)
4. Al-Hadeethi, Y.; Sayyed, M.I.; Rammah, Y.S. Fabrication, optical, structural and gamma radiation shielding characterizations of  $\text{GeO}_2\text{--}\text{PbO}\text{--}\text{Al}_2\text{O}_3\text{--}\text{CaO}$  glasses. *Ceram. Int.* **2020**, *46*, 2055–2062. [\[CrossRef\]](#)
5. Chen, T.-Y.; Rautiyal, P.; Vaishnav, S.; Gupta, G.; Schlegel, H.; Dawson, R.; Evans, A.; Kamali, S.; Johnson, J.; Johnson, C.; et al. Composition-structure-property effects of antimony in soda-lime-silica glasses. *J. Non-Cryst. Solids* **2020**, *544*, 120184. [\[CrossRef\]](#)
6. D'Souza, A.N.; Prabhu, N.S.; Sharmila, K.; Sayyed, M.I.; Somshekarappa, H.M.; Lakshminarayana, G.; Mandal, S.; Kamath, S.D. Role of  $\text{Bi}_2\text{O}_3$  in altering the structural, optical, mechanical, radiation shielding and thermoluminescence properties of heavy metal oxide borosilicate glasses. *J. Non-Cryst. Solids* **2020**, *542*, 120136. [\[CrossRef\]](#)
7. Rahman, N.A.A.; Matori, K.A.; Zaid, M.H.M.; Zainuddin, N.; Ab Aziz, S.; Khiri, M.Z.A.; Jalil, R.A.; Jusoh, W.N.W. Fabrication of Alumino-Silicate-Fluoride based bioglass derived from waste clam shell and soda lime silica glasses. *Results Phys.* **2019**, *12*, 743–747. [\[CrossRef\]](#)
8. Almasri, K.A.; Sidek, H.A.A.; Matori, K.A.; Zaid, M. Effect of sintering temperature on physical, structural and optical properties of wollastonite based glass-ceramic derived from waste soda lime silica glasses. *Results Phys.* **2017**, *7*, 2242–2247. [\[CrossRef\]](#)
9. Khalil, E.; ElBatal, F.; Hamdy, Y.; Zidan, H.; Aziz, M.; Abdelghany, A.M. Infrared absorption spectra of transition metals-doped soda lime silica glasses. *Phys. B Condens. Matter* **2010**, *405*, 1294–1300. [\[CrossRef\]](#)
10. Singh, S.; Kumar, A.; Singh, D.; Singh, K.; Mudahar, G.S. Barium–borate–flyash glasses: As radiation shielding materials. *Nucl. Instrum. Methods Phys. Res. B* **2008**, *266*, 140–146. [\[CrossRef\]](#)
11. Manohara, S.; Hanagodimath, S.; Gerward, L. Photon interaction and energy absorption in glass: A transparent gamma ray shield. *J. Nucl. Mater.* **2009**, *393*, 465–472. [\[CrossRef\]](#)
12. Kurtulus, R.; Kavaz, T. Investigation on the physical properties, shielding parameters, glass formation ability, and cost analysis for waste soda-lime-silica (SLS) glass containing SrO. *Radiat. Phys. Chem.* **2020**, *176*, 109090. [\[CrossRef\]](#)
13. Sallam, O.; Madbouly, A.; Elalaily, N.; Ezz-Eldin, F. Physical properties and radiation shielding parameters of bismuth borate glasses doped transition metals. *J. Alloys Compd.* **2020**, *843*, 156056. [\[CrossRef\]](#)



14. Al-Hadeethi, Y.; Sayyed, M. Analysis of borosilicate glasses doped with heavy metal oxides for gamma radiation shielding application using Geant4 simulation code. *Ceram. Int.* **2019**, *45*, 24858–24864. [\[CrossRef\]](#)
15. Sayyed, M.; Ati, A.A.; Mhareb, M.; Mahmoud, K.; Kaky, K.M.; Baki, S.; Mahdi, M. Novel tellurite glass (60-x)TeO<sub>2</sub>-10GeO<sub>2</sub>-20ZnO-10BaO-xBi<sub>2</sub>O<sub>3</sub> for radiation shielding. *J. Alloys Compd.* **2020**, *844*, 155668. [\[CrossRef\]](#)
16. Prasad, R.N.A.; Venkata Siva, B.; Neeraja, K.; Krishna Mohan, N.; Rojas, J.I. Effect of modifier oxides on spectroscopic and optical properties of Pr<sup>3+</sup> doped PbO-R<sub>2</sub>O<sub>3</sub>-WO<sub>3</sub>-B<sub>2</sub>O<sub>3</sub> glasses (with R<sub>2</sub>O = Sb<sub>2</sub>O<sub>3</sub>, Al<sub>2</sub>O<sub>3</sub>, and Bi<sub>2</sub>O<sub>3</sub>). *J. Lumin.* **2021**, *230*, 117666. [\[CrossRef\]](#)
17. Kaky, K.M.; Sayyed, M.; Ati, A.A.; Mhareb, M.; Mahmoud, K.; Baki, S.; Mahdi, M. Germanate oxide impacts on the optical and gamma radiation shielding properties of TeO<sub>2</sub>-ZnO-Li<sub>2</sub>O glass system. *J. Non-Cryst. Solids* **2020**, *546*, 120272. [\[CrossRef\]](#)
18. Kaky, K.M.; Sayyed, M.; Mhareb, M.; Abdalsalam, A.H.; Mahmoud, K.; Baki, S.; Mahdi, M. Physical, structural, optical and gamma radiation attenuation properties of germanate-tellurite glasses for shielding applications. *J. Non-Cryst. Solids* **2020**, *545*, 120250. [\[CrossRef\]](#)
19. Rammah, Y.; El-Agawany, F.; Mahmoud, K.; Novatski, A.; El-Mallawany, R. Role of ZnO on TeO<sub>2</sub>.Li<sub>2</sub>O.ZnO glasses for optical and nuclear radiation shielding applications utilizing MCNP5 simulations and WINXCOM program. *J. Non-Cryst. Solids* **2020**, *544*, 120162. [\[CrossRef\]](#)
20. Makishima, A.; Mackenzie, J.D. Direct calculation of Young's modulus of glass. *J. Non-Cryst. Solids* **1973**, *12*, 35–45. [\[CrossRef\]](#)
21. Makishima, A.; Mackenzie, J.D. Calculation of Bulks modulus, Shear modulus and Piosson's ratio of glass. *J. Non-Cryst. Solids* **1975**, *17*, 147–157. [\[CrossRef\]](#)
22. X-5 Monte Carlo Team. *MCNP-A General Monte Carlo N-Particle Transport Code, Version 5*; LA-CP-03-0245; Los Alamos Controlled Publication: Los Alamos County, NM, USA, 2003.
23. Abouhaswa, A.; Sayyed, M.; Mahmoud, K.; Al-Hadeethi, Y. Direct influence of mercury oxide on structural, optical and radiation shielding properties of a new borate glass system. *Ceram. Int.* **2020**, *46*, 17978–17986. [\[CrossRef\]](#)
24. Divina, R.; Marimuthu, K.; Mahmoud, K.; Sayyed, M. Physical and structural effect of modifiers on dysprosium ions incorporated boro-tellurite glasses for radiation shielding purposes. *Ceram. Int.* **2020**, *46*, 17929–17937. [\[CrossRef\]](#)
25. Mahmoud, K.; Lacomme, E.; Sayyed, M.; Özpölat, Ö.F.; Tashlykov, O. Investigation of the gamma ray shielding properties for polyvinyl chloride reinforced with chalcocite and hematite minerals. *Heliyon* **2020**, *6*, e03560. [\[CrossRef\]](#)
26. El Abd, A.; Mesbah, G.; Mohammed, N.M.A.; Ellithi, A. A simple Method for Determining the Effective Removal Cross Section for Fast Neutrons. *J. Radiat. Nucl. Appl.* **2017**, *2*, 53–58. [\[CrossRef\]](#)
27. Inaba, S.; Fujino, S.; Morinaga, K. Young's Modulus and Compositional Parameters of Oxide Glasses. *J. Am. Ceram. Soc.* **1999**, *82*, 3501–3507. [\[CrossRef\]](#)
28. Bloomfield, L. *How Things Work: The Physics of Everyday Life*, 2nd ed.; Wiley: New York, NY, USA, 2001.
29. Rammah, Y.; Mahmoud, K.; Sayyed, M.; El-Agawany, F.; El-Mallawany, R. Novel vanadyl lead-phosphate glasses: P<sub>2</sub>O<sub>5</sub>-PbO-ZnO Na<sub>2</sub>O-V<sub>2</sub>O<sub>5</sub>: Synthesis, optical, physical and gamma photon attenuation properties. *J. Non-Cryst. Solids* **2020**, *534*, 119944. [\[CrossRef\]](#)
30. Berger, M.J.; Hubbel, J.H. XCOM: Photon Cross Sections Database, Gaithersburg, MD 20899, USA. 1987. Available online: <http://physics.nist.gov/xcom> (accessed on 15 October 2020).
31. Yorgun, N.Y.; Kavaz, E.; Tekin, H.; Sayyed, M.; Ozdemir, O.F.; Yildiz, N. Borax effect on gamma and neutron shielding features of lithium borate glasses: An experimental and Monte Carlo studies. *Mater. Res. Express* **2019**, *6*, 115217. [\[CrossRef\]](#)